NJC

ROYAL SOCIETY OF CHEMISTRY

PAPER

View Article Online
View Journal | View Issue



Cite this: *New J. Chem.*, 2025, **49**, 5707

# Azadirachtin-based formulation in combination with mesoporous silica materials as a plague control agent†

Míriam Benítez,[a] Jamal El Haskouri,[b] Carlos Montesinos,[c] Pedro Amorós *[b] and José Vicente Ros-Lis *[a]

Azadirachtin is the most important active ingredient of neem oil, a standout product among essential oils. These substances are an interesting family of active products because of their non-toxicity to vertebrates, their specificity against certain pests and the fact that they do not induce resistance. The encapsulation of essential oils and insecticides of natural origin is a widely used strategy to improve their properties. In this work, the ability of silica materials with different topologies and functionalizations to encapsulate and release neem oil and an azadirachtin-based formulation was evaluated. A material containing titanium has also been prepared as a potential protector against UV radiation. It is observed that the presence of the textural pores of the UVM-7 material favors the capture and modulates the release. On the other hand, the mesopores offer a minor contribution. Regarding functionalization, coatings with amine and alkane groups were tested, which did not improve their properties. The UVM-7 material with and without titanium loaded with Zenith A26 was tested in the field against *E. banksi* in citrus, showing values of incidence and severity close to the conventional treatment with citrulline. Conversely the presence of titanium offered only a minor improvement. Thus, these types of materials could be an interesting approach towards more sustainable agriculture.

Received 31st January 2025,
Accepted 25th February 2025

DOI: 10.1039/d5nj00431d

rsc.li/njc



## Introduction

The uncontrolled use of agrochemicals has led to serious health and environmental problems.[1–3] Restrictive regulations have been adopted, and dangerous chemicals have been banned from the market, at least in developed countries. In addition, the appearance of resistances to pesticides has been observed. This lack of tools for the control of pathogens is coupled with an increase in the entry of invasive insects into Europe because of the increase in international trade in ornamental and cultivated plants.[4] Therefore, due to the emergence of new pests and the restriction of raw materials, it is necessary to provide new tools to develop a long-term sustainable strategy.

Biopesticides have emerged as an alternative to synthetic chemicals. They are defined as agents used for the management of agricultural pests based on microorganisms or natural products with minimal environmental impact.[5,6] The main advantages of applying biopesticides as natural compounds compared to conventional pesticides are: (i) lower toxicity; (ii) affecting only the target pest; (iii) very potent in very small amounts; (iv) rapid decomposition; and (v) low exposure, with almost no pollution problems.[7] Among biopesticides, essential oils (EOs) are remarkable raw materials.[8,9]

EOs are volatile secondary metabolites of many plants that play an important role in host defense mechanisms against biotic or abiotic stress.[10] In their application as phytopathogens, oils cause the death of insects and mites.[11–14] Essential oils of *Rosmarinus officinalis* and *Salvia officinalis* gave positive results by reducing larval emergence of *Tetranychus urticae*.[15] On the other hand, oils have been cited in numerous studies as agents capable of reducing the transmission of various plant viruses by their insect vectors.[7,11] Indirectly, essential oils can help plants fight insects due to their phytofortifying and biostimulant activities.

Neem oil is a vegetable oil extracted from the fruits and seeds of the neem tree (*Azadirachta indica* A. Juss),[16] used for centuries for pest control in agricultural crops.[17] The extracts

[a] *REDOLí research group, Instituto Interuniversitario de Investigación de Reconocimiento Molecular y Desarrollo Tecnológico (IDM), Universitat de València, C/Dr Moliner 50, 46100, Burjassot, Spain. E-mail: J.Vicente.Ros@uv.es*
[b] *Institut de Ciència dels Materials (ICMUV), Universitat de València, C/Catedrático José Beltrán 2, Paterna, 46980, Valencia, Spain. E-mail: pedro.amoros@uv.es*
[c] *Asociación Valenciana de Agricultores (AVA-ASAJA), C/Guillem de Castro, 79, 46008, Valencia, Spain*

† Electronic supplementary information (ESI) available. See DOI: https://doi.org/10.1039/d5nj00431d

obtained from its seed contain various bioactive agents against fungi and insects and are used for health applications.[18] The most potent is the nortriterpenoid known as azadirachtin for its insecticidal activity and quantity present in neem seeds.[19–21] Extracts with a high concentration of azadirachtin could be the precursors of a new generation of insecticidal, fungicidal, acaricidal and crop protection products without contaminating the environment and interrupting sperm production in males of certain species.[22–25] A study carried out on mandarin seedlings shows that azadirachtin has obtained satisfactory results in terms of mortality in individuals of *Phyllocnistis citrella*.[26]

Despite all the advantages listed above, the direct application of essential oils is not entirely effective because they can have little permanence and many of them degrade easily because of temperature or solar radiation. It is at this point that nanotechnology, and specifically the use of nanomaterials capable of encapsulating EOs, can be advantageous.[27–30] Nanomaterials have appeared as an interesting alternative for the design of therapeutic and theragnostic applications.[31–34] The application of nanotechnology in biopesticide formulations and delivery has the potential to revolutionize this field and make agribusiness greener and safer.

Nanopesticides consist of organic or inorganic structures that act as a vehicle for active ingredients such as EOs. Among organic nanomaterials, biopolymers stand out, and among those of an inorganic nature, metals and oxides. Nanoemulsions of crude neem and citronella have been used, along with neem gum nanoformulations that have shown remarkable larvicidal activity against lepidoptera such as *Helicoverpa armigera*, *Spodoptera litura* and *Plutella xylostella*, among others. Controlled neem oil release systems based on organic supports such as carbohydrates and polymers have limitations such as a high degree of water retention that can accelerate the hydrolysis and release of neem compounds.[35–41] An alternative is based on the use of mesoporous silicas.[42–45] Silica-based supports have important additional advantages to their low or no toxicity, such as the possibility of achieving good shape and size control, and high thermal and chemical stability. It has the potential to protect from evaporation and degradation and enhance biocidal action. The modulation of the interaction between azadirachtin and the silica surface, as well as its encapsulation in the pores, allows for the establishment of slow and sustained controlled release profiles over time.

For all these reasons, we hypothesize that nanomaterials can enhance the activity of azadirachtin-based formulations, giving rise to an improved nanoinsecticide, potentially for use in organic farming that helps farmers maintain the productivity of their crops in an increasingly complicated environment due to climate change.

# Experimental

## Materials and methods

**Reagents.** All the synthesis reagents were analytically pure and were used without further purification as received from Sigma-Aldrich Chemistry, Scharlab S.L. and Merck.

**Instrumentation.** All solids were characterized by X-ray powder diffraction (XRD) at low angles (Bruker D8 Advance Diffractometer) using a monochromatic Cu Kα source operating at 40 kV and 40 mA. Patterns were collected in steps of 0.02° (2$\theta$) over the angular range 1–10.0° (2$\theta$) for 3 s per step. Transmission electron microscopy (TEM) images were taken with a JEOL-2100F microscope operating at 200 kV. Samples were dispersed in ethanol and placed onto a holey carbon film supported on a Cu microgrid and left to dry before observation. The Si and Ti content was determined by energy dispersive X-ray spectroscopy EDX analysis using a scanning electron microscope (Philips – SEM-XL 30). The Si/Ti molar ratio value was averaged from EDX data. Nitrogen adsorption–desorption isotherms were recorded on a Micromeritics TriStar Plus II automated analyzer. The samples were degassed *in situ* at 120 °C and $10^{-6}$ Torr for 15 h prior to analysis. Specific surface areas were calculated from the adsorption data within the low-pressure range using the Brunauer–Emmett–Teller (BET) model. Pore sizes and pore volumes were determined following the Barrett–Joyner–Halenda (BJH) model on the adsorption branch. Thermogravimetric analysis (TGA) was performed with a TA55/550 instrument equipped with a Furnace EGA under a dry air flow at a heating rate of 10 °C $min^{-1}$ up to 1000 °C. Determination of the particle size has been carried out by using a Malvern Mastersizer 2000 equipment. The measurement process was conducted in triplicate, and the resulting values were then averaged to ensure the robustness and reliability of the results. FTIR spectra were recorded using a PerkinElmer attenuated total reflectance (ATR) single bounce diamond accessory.

### Synthesis, functionalization, and loading of the materials.

**Stöber material (Stöber)[46].** 28.6 mL of $H_2O$, 68 mL of ethanol and 3.3 mL of $NH_4OH$ were stirred for 10 minutes at room temperature. 5.9 mL of tetraethylorthosilicate (TEOS) was added and the resulting solution was aged at room temperature for 48 h. The resulting mesostructured powder was separated through centrifugation, washed with ethanol, and dried at 80 °C overnight.

**Porous Stöber material (NPS)[47].** 11 mL of TEOS and 25 mL of triethanolamine ($TEAH_3$) were heated at 140 °C. The resulting solution was cooled to 120 °C, 4.5 g of cetyltrimethylammonium bromide (CTABr), 450 mL of water and 250 mL of ethanol were added. After a few minutes, a white suspension resulted. This mixture was aged at 40 °C for 48 h. The resulting mesostructured powder was separated through centrifugation, washed with ethanol, and dried at 80 °C overnight. Finally, the surfactant was removed from the as-synthesized material by calcination at 550 °C for 6 h.

**UVM-7[48].** 1 L of deionized water was added to 412 mL of the atrane mixture containing Si (263 mL of TEAH3, 137 mL of TEOS, and 45 g of CTABr). The mixture was stirred until homogeneity was achieved, then it was placed into the microwave oven cavity and irradiated for 12 minutes at 800 W until the gel was formed. The white solid obtained was filtered, washed with water and ethanol, dried in an oven at 80 °C overnight and calcined at 550 °C for 5 h to remove the CTABr surfactant.

 

**Ti-UVM-7[49].** 1 L of deionized water was added to 412 mL of the atrane mixture containing Si and Ti (263 mL of TEAH3, 131 mL of TEOS, 8 mL of tetrabutyl orthotitanate ($Ti(OBut)_4$), and 45 g of CTABr). The mixture was stirred until homogeneity was attained, then placed into the microwave oven cavity and irradiated for 12 minutes at 800 W until the gel was formed. The white solid obtained was filtered, washed with water and ethanol, dried in an oven at 80 °C overnight and calcined at 550 °C for 5 h to remove the CTABr surfactant.

**Functionalization with amines.** 2.5 g of substrate (UVM-7, Ti-UVM-7 or fumed silica (FS)) were added to a 150 mL acetonitrile solution containing 3,5 mL of 3-(aminopropyl)-triethoxysilane (APTES) and placed into the microwave oven cavity and irradiated for 16 minutes at 200 W. The resulting solid was filtered, washed with acetonitrile, and dried in an oven at 80 °C overnight.

**Functionalization with methyl groups.** 1 g of substrate (UVM-7, Ti-UVM-7 or FS) was added to a 50 mL acetonitrile solution containing 0.76 mL of chlorotrimethylsilane ($ClSiMe_3$) and stirred for 24 h at room temperature. The resulting solid was filtered, washed with acetonitrile, and dried at 80 °C overnight.

**Loading with Zenith A26.** 0.4 g of the silica material, 4.3 mL of Zenith A26 and 2 mL of DMSO were stirred for 24 h at room temperature. After this, the material was filtered and washed with ethanol.

**Loading with neem oil.** 0.5 g of the silica material, 0.5 mL of neem oil and 15 mL of $CHCl_3$ were stirred for 24 h at room temperature. After this, the material was filtered and washed with $CHCl_3$.

**Loading with azadirachtin.** 0.5 g of the silica material, 30 mg of azadirachtin (98%) and 10 of acetonitrile were stirred for 24 h at room temperature. After this, the material was filtered and washed with $CHCl_3$.

**Loading for the field tests.** 11.8 g of silica-based support loaded with the commercial insecticide Zenith A26 were added to every liter of water solution.

### Release studies

50 mg of silica product loaded with Zenith A26 were placed on a heating plate at 36 °C, and the release of Zenith A26 was measured by a weight difference at different times (1, 3, 24 and 48 h).

### Evaluation of the biocidal activity

The biocidal evaluation was performed in the Finca Sinyent. An experimental farm owned by the Asociación Valenciana de Agricultures (AVA-ASAJA). The assays with *Eutetranychus banksi* were developed using 8 years old orange trees of the Chislett variety. The treatments were applied in four lines occupying 970 $m^2$. They included 4 treatments with 5 replicas, 5 subsamples per repetition: 25 total data per treatment. List of treatments: conventional (citrulline: paraffin oil 79% from SIPCAM IBERICA) (E1), Zenith A26 (E2), Zenith A26 loaded UVM-7 (E3), and Zenith A26 loaded Ti-UVM-7 (E4). Also, it included a control thesis without treatment (E0). A randomized assignment was applied for the thesis distribution. The elemental plot size for each replica was 3 trees and an area of 33 $m^2$. The doses of the product were 75 mL $hL^{-1}$, except citrulline that was applied at 1500 mL $hL^{-1}$, and doses of 2000 L $ha^{-1}$ were applied to achieve a correct wetting of both sides of the leaf. For the evaluation, 25 leaves per plot and number of larval stages (L1 and L2) were randomly selected. The evaluation was done 3 and 7 days after application.

### Data analysis

In biocidal activity studies, incidence denotes the percentage of leaves with the presence of plague, and severity denotes the number of larvae motile mites (*E. banski*) per leaf. Agriculture Research Management Software was used for data analysis and statistics. A significance level of $p = 0.05$ was used unless otherwise stated in the text.

## Results and discussion

### Effect of the silica topology

Silica materials are especially versatile due to their relatively inert chemical behavior and their ability to obtain particles with different sizes, morphology, pore structures, and surface functionalizations. As the first step, the effect of the topology of the material on its adsorption/desorption capacities was evaluated. Three materials with different morphologies and porosities were prepared for the purpose of evaluating the effect of these characteristics on the absorption/desorption capacity of essential oil and its biocidal activity. Its appearance and morphology can be seen in Fig. 1. The Stöber-type particles are characterized by their spherical shape in the nanometric range and homogeneous particle size. In our case, we have prepared dense particles (without pores) and mesoporous particles (NPS) (around 2 nm). Poreless Stöber particles allow the effect of surface adsorption to be assessed, while mesoporous particles illustrate the effect of mesopores. The family of mesoporous materials also includes UVM-7 materials, made up of small primary mesoporous particles aggregated between them, leaving a textural pore (around 40 nm). The aggregated particles of UVM-7 are smaller than the Stöber particles, therefore they have a smaller pore length which can influence the loading and diffusion of host species. In addition, fumed silica (FS) an amorphous, white, commercial material with small particle size (see Fig. 1) with its corresponding high surface area and high surface activity has been evaluated.

The topological properties can be observed in greater detail, thanks to the measurement of the $N_2$ adsorption/desorption isotherms (see Table 1). As expected, both mesoporous materials (NPS and UVM-7) present a well-defined mesopore (around 2.5 nm) associated with the template effect of the surfactant micelles, which is associated with a high surface area, around $>800$ $m^2$ $g^{-1}$. It is evident that compared to the non-porous FS support, the presence of mesopores considerably increases the surface area. Furthermore, a larger pore of textural nature is also observed in both silicas. However, the significance and

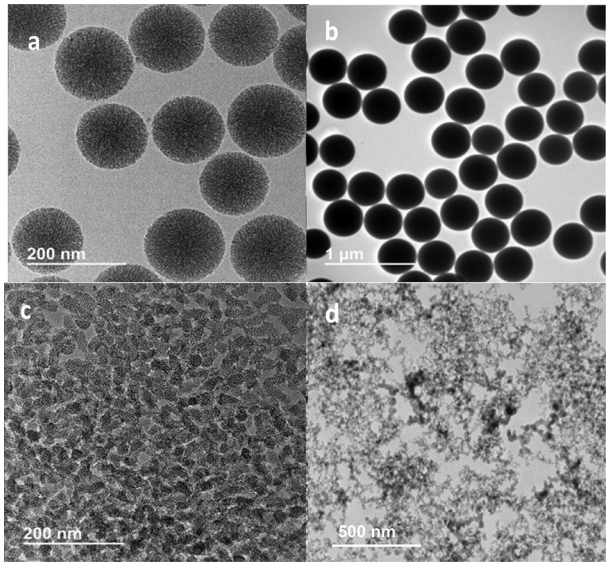


Fig. 1 Electronic microscopy (TEM) images. (a) Porous Stöber particles (NPS), (b) nonporous Stöber particles, (c) UVM-7, (d) fumed silica.

Table 1 BET surface area and mesopore size of the different prepared materials

| Material | Area ($m^2$ $g^{-1}$) | Mesop. diam. (nm) | Mesop. vol. ($cm^3$ $g^{-1}$) | Text pore diam. (nm) | Text vol. ($cm^3$ $g^{-1}$) |
|---|---|---|---|---|---|
| Stober | 18 | — | — | — | — |
| NPS | 1248 | 2.5 | 1.01 | 31.1 | 0.4 |
| UVM-7 | 860 | 2.6 | 0.66 | 41.7 | 2.4 |
| FS | 373 | — | — | | |

subsequent relevance of this large pore for the capture of host species vary markedly between the two materials. In the case of UVM-7, the large mesopore (with a diameter between meso and macropores) has a significant associated pore volume associated to its characteristic material's architecture. This additional porosity is attributed to the voids between partially condensed primary nanoparticles that form aggregates, as evidenced by TEM images. In contrast, the NPS material's textural porosity is associated with a very low residual pore volume. Indeed, in NPS silica, which consists of individual spherical particles of uniform size, this porosity is due to certain voids that define the particles when packed in powder form. In the opposite extreme, we find the non-porous Stöber particles, which, as expected, have the smallest surface area of all materials (only 18 $m^2$ $g^{-1}$), corresponding to the outer surface of the spheres. In this instance, the larger size of the particles does not generate cavities when packed, which can be filled with nitrogen by capillarity. With intermediate values, pyrogenic silica (FS) has an area of 373 $m^2$ $g^{-1}$. In this case, diffusion of the host species is favored due to the absence of intrinsic porosity. Even if a certain textural porosity associated with the gaps between particles is considered, this material contains relatively large pore size, in the range of macropores. For the purposes of this work, diffusion through FS is not a drawback and we can consider that it is a surface adsorption in an unconfined space.

In the case of mesoporous materials synthesized with the aid of surfactants (NPS and UVM-7), the intra-particle pore arrangement presents a certain order, which is evidenced by the presence of a low-angle X-ray diffraction peak corresponding to the family of planes (100) (Fig. 2). In addition to this strong signal, the diffractograms of the three materials show a very broad signal (shoulder to the right of the main peak) which can be assigned to the overlapping reflections (110) and (200). The absence of additional well-resolved signals in the XRD pattern (as in the MCM-41 materials) indicates a distorted hexagonal pore organisation. However, it should be noted that while the existence of mesopores (accessible to the guest species) could be of great relevance for the tested applications, the order between mesopores does not provide any additional advantage. In the case of UVM-7, the peak can be found at 2.1° ($2\theta$), while in the mesoporous Stober particles (NPS), the peak appears at 2.4°($2\theta$), which indicates a smaller cell size. As the intra-particle mesopore size is comparable for both materials, the UVM-7 material has a larger pore wall thickness ($a_0 = 2d_{100}/3^{1/2}$; wall thickness = $a_0$ − pore size = 2.08 nm) than NPS (1.75 nm), indicating enhanced thermal stability and a prolonged degradation time for the UVM-7 support.

As an initial test to evaluate the adsorption capacity of the different materials, Zenith A26 (A26) was used as the active material. A26 is a commercial formulation containing 2.6% azadirachtin. Considering a practical application, the enhancement of the commercial formulation offers more promising prospects for implementation, as it is a product that is currently available in the market and has successfully met all regulatory criteria. As can be seen in Fig. 3, the topology of the material has a great influence on the absorption capacity. It is interesting to note that the two materials which demonstrate a lower absorption capacity are those composed of Stöber particles (both massive and porous). The presence of mesopores (NPS) has been shown to generate an increase in adsorption capacity; however, the minor discrepancy observed between the two silicas indicates that mesopores within NPS do not possess a

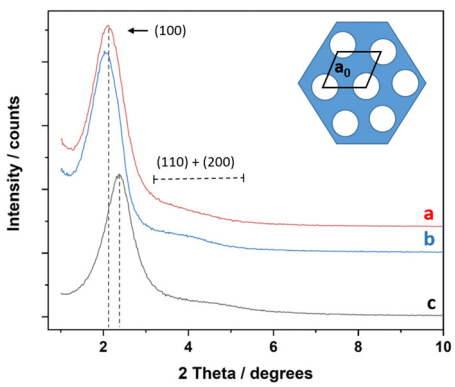


Fig. 2 Low-angle XRD patterns of (a) UVM-7, (b) Ti-UVM-7 and (c) NPS supports.

 

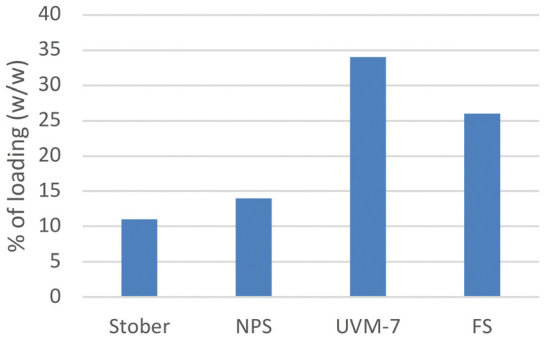


Fig. 3 Amount of Zenith A26 loaded on the silica materials.

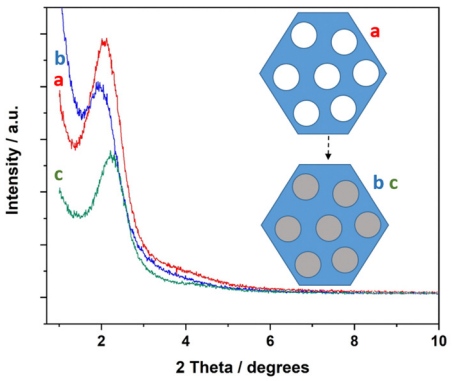


Fig. 4 Low-angle XRD patterns of (a) UVM-7, (b) UVM-7 loaded with Zenith A26 and (c) with neem oil.

substantial adsorption capacity. It can thus be concluded that the majority of the loading must occur on the material's surface. The disparities detected can be attributed to the roughness induced by mesopore entrances. Azadirachtin has a size of 1.3 nm, which is smaller than the BJH mesopore size. However, the small size of the mesopores and their length (in principle similar to the diameter of the particles, *ca.* 170 nm) probably hinder the adsorption and necessary diffusion of azadirachtin to fill the pores (which could generate blockage of these) despite the high contact time used in the synthesis. Conversely, materials characterized by larger textural pores, such as UVM-7 with large mesopores and non-porous FS, exhibited a higher absorption capacity of up to 33% (w/w), irrespective of the presence or absence of intraparticle mesopores. As previously mentioned, the total surface area, which is primarily associated with the mesoporous structure, does not appear to be a key factor. Nonetheless, large textural pores (diameter greater than 40 nm) are readily accessible and may function as reservoirs, thereby facilitating the preferential accumulation of the active principle.

Although mesopores seem to offer a minor contribution in Stober materials, in a material such as UVM-7, with small pore length (maximum values of the primary particle size, *ca.* 40 nm), a greater ease of diffusion of azadirachtin can be expected, which could at least be incorporated into the mesopore entrances. This finding is consistent with the hypothesis that the UVM-7 material, which combines the largest volume of large mesopores, the slightly larger intra-particle mesopore diameter and the shortest length, is the material with the highest absorption capacity.

The $N_2$ adsorption/desorption studies of UVM-7 loaded with A26 demonstrate a substantial reduction (compared to uncharged silica) in the surface area (225 $m^2\ g^{-1}$) and in the intraparticle and textural mesopore volumes, with values of 0.19 and 1.38 $cm^3\ g^{-1}$, respectively. The reduction in volume is evident for both types of mesopore, with a higher percentage observed in the intra-particle mesopore (80%) compared to the textural one (63%). Nevertheless, the most significant reduction in volume is observed in the larger mesopore, with a decrease from 2.4 to 1.38 $cm^3\ g^{-1}$. On the other hand, the XRD pattern of UVM-7 silica loaded with A26 shows a clear decrease in signal intensity at low angles relative to the unloaded material. This feature is consistent with phase cancellation, which can only be explained if the active ingredient penetrates the intra-particle mesopores (to a greater or lesser extent considering the possible blocking of mesopores) (Fig. 4). A similar evolution of the relative intensity of the (100) signal is observed when the support is loaded with neem oil. In summary, the active substance can penetrate the intra-particle mesopores or at least lodge at the entrance of the mesopores but is likely to be mostly located on the outer surface and especially in the large textural pores. Considering the lower loading capacity and the high cost of preparation of Stöber particles, the following tests were carried out only with materials containing large mesopores or macropores.

Apart from the utilization of silica materials as support for commercial formulation (A26), the adsorption capacity of neem oil and azadirachtin, its active ingredient, was evaluated. The concentration of azadirachtin in seeds varies from 430 to 3830 ppm depending on the seeds quality and the extraction method.[50] We observed that the adsorption capacity in the case of neem oil (31 and 26% for UVM-7 and FS, respectively) is practically the same as that observed for A26, which suggests that absorption would also occur on the surface and large mesopore/macropore of the material. In fact, in the case of UVM-7 as the support, a decrease in BET area and pore volumes, as well as in peak intensity (100) at low angles, is also observed. Conversely, the absorption of pure azadirachtin is lower under our experimental conditions (16 and 8% for UVM-7 and FS, respectively). Despite these lower concentrations, it is noteworthy that in relation to the percentage of active substance in the loaded compound, the azadirachtin content would exceed that of A26 or neem oil in this final case. This suggests that mesoporous silica materials may serve not only to encapsulate commercial formulations but also to carry the essential oil or active substance.

To study the effect of the support on the release, the weight loss of mesoporous materials loaded with Zenith A26 was tested. As can be seen in Fig. 5, the weight loss of loaded materials is significantly lower than that of pure A26 (12–32%). In the case of fumed silica, the slowing effect increases with time and is mainly observed for extended periods (24 hours).

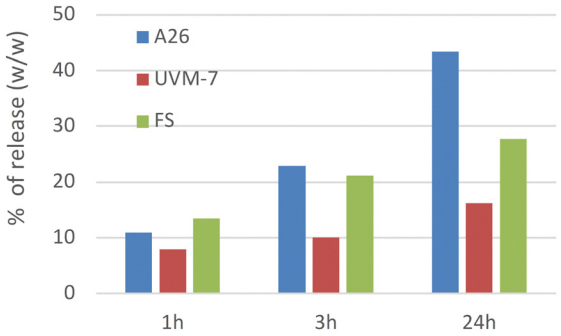


Fig. 5 Evolution of the Zenith A26 release to the air at different times. A26: pure Zenith A26 product.

However, in the case of UVM-7 silica, the slowing effect on the release of A26 is more pronounced and occurs even at very short times (1 hour). In consideration of the obtained results, it can be indicated that the release mechanism of the A26 agent from the charged supports into the surrounding atmosphere is governed by capillary forces. Consequently, the intrinsic bimodal porosity of the UVM-7 material, in comparison with the nonporous nature of the FS, generates a retention effect of A26 that is approximately twice as high, thereby extending its lifetime. However, it should be noted that the portion of active ingredient entrapped within the intraparticle mesopores or at their entrances will exhibit higher resistance when it comes to its elimination. It appears that the optimal combination of large-meso/macroporosity with mesopores (intraparticle) and a high surface area may be the most effective strategy to ensure the prolonged permanence of the product.

### Effect of functionalization

Since the adsorption and release of substances is a phenomenon that may depend on the nature of the surface of the material, the UVM-7 material was functionalized with various organic groups. Specifically, amino (U-NH2) and methyl (U-CH3) groups were incorporated. The first has a polar character, the ability to form hydrogen bonds and potential for protonation. The second confers a hydrophobic nature to the surface. The percentages of functionalization calculated from TGA are 2.1 mmol (g of silica)$^{-1}$ for U-NH2 to 3.2 mmol (g of silica)$^{-1}$ for U-CH3. In addition, the incorporation of the organic arms was verified by FTIR (Fig. S1, ESI†). As expected, the IR spectra are dominated by the absorption bands of the silica (major component). However, small signals that can be ascribed to N–H bending (*ca.* 1525 cm$^{-1}$) and C–H stretching (*ca.* 2930 cm$^{-1}$) vibrations are clearly detectable for the APTES-functionalized supports. In these solids, N–H stretching vibrations are not clearly detected due to overlapping with the typical O–H stretching vibrations of water molecules. In the case of the $ClSiMe_3$-modified solids, no bands are detected around 1525 cm$^{-1}$; however, the bands associated with C–H stretching vibrations (due to $CH_3$ groups) are detected more intensely than in the APTES-modified derivatives. It can be observed that functionalization decreases the loading capacity of the supports with A26 by more than 50% (see Table 2). Since we have tested two

Table 2 Loading of and release kinetics of the functionalized supports in contact with Zenith A26

| | | % of A26 load released | | |
|---|---|---|---|---|
| Material | % loading | 1 h | 3 h | 24 h |
| UVM-7 | 34 | 8 | 10 | 16 |
| U-NH2 | 13 | 61 | 78 | 104 |
| U-CH3 | 12 | 50 | 56 | 56 |

diverse coatings, a hydrophilic (U-NH2) and hydrophobic surface (U-CH3), and observed a similar effect in both cases, we can assign this behavior to the reduction in the pore void associated to the organic coating added during functionalization. The rate of release is also widely affected by functionalization. In the case of the material coated with amino groups, the release is substantially faster than in the non-functionalized material (it increases from 8 to 61% in one hour) and continues during the test reaching a complete release in 24 h. In the case of the material with methyl groups, the release is also faster than in the non-functionalized material (50%), but a significant part of the material is captured within the matrix, probably due to hydrophobic interactions, with only a small weight loss observed in the following hours. From these data, considering the degree of charge, release kinetics, and its greater ease of synthesis, the non-functionalized UVM-7 material could be most suitable for a practical application. In any case, customised formulations could be made by combining different silica-based carriers (with different functionalisations) to achieve specific release profiles.

### Ti containing UVM-7 material

As mentioned above, silica topology and functionalization have great potential to modify the loading capacity and release of an azadirachtin-containing formulation. The porous system can act by protecting its contents from the outside. In addition, the composition of the substrate can also be modified with agents that protect the active substances from degradation induced by ultraviolet light. Titanium oxide is widely used for this purpose. Therefore, a material similar to UVM-7 but containing Ti was synthesized from a nominal Si : Ti ratio of 25 : 1. EDX analysis indicates that the final solid has been enriched in Ti, as evidenced by the Si/Ti molar ratios determined by EDX, which are slightly lower (Si : Ti = 17 : 1) than the stoichiometric values added during the synthesis (nominal values). It is acknowledged that the materials can be described as mixtures of $SiO_2$ and $TiO_2$ oxides, and it is well established that the solubility of $SiO_2$ is higher than that of $TiO_2$. Therefore, the Ti enrichment can be attributed to the partial dissolution of silica. In our case, we have used the atrane route for synthesis, which allows the preparation of UVM-7 mesoporous materials containing other elements in high proportions without a significant modification of their structure. The prepared material (Ti-UVM-7) has the same characteristics as pure (Ti free) silica UVM-7: an architecture based on aggregates of small mesoporous particles with an ordered pore system, an XRD peak at $2\theta = 2.1^\circ$, a surface area of 885 m$^2$ g$^{-1}$ and the presence of a bimodal pore system of 2.4 and 42.4 nm with pore volumes of 0.70 and 1.23 cm$^3$ g$^{-1}$.

 

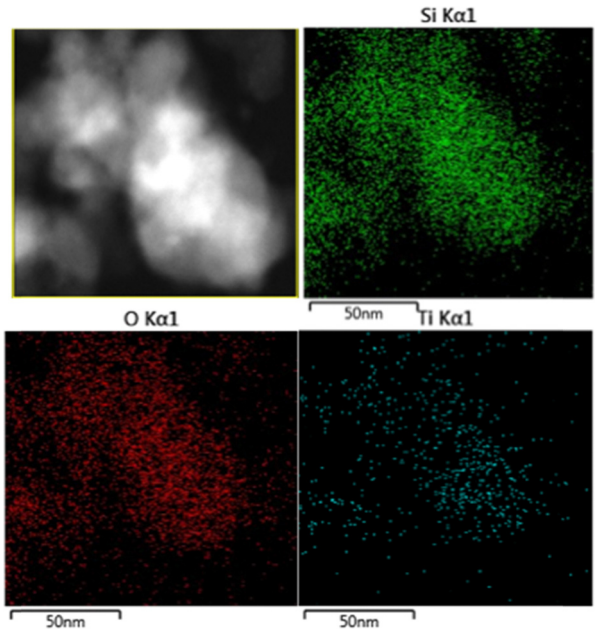


Fig. 6 EDX-SEM images of the Ti-UVM-7 material.

If we look at the X ray fluorescence images obtained in the SEM equipment, the titanium within the material is homogeneously distributed without generating segregated clusters (Fig. 6). In previous work, it was observed that this type of material can offer an SPF of 4.[49]

### Particle size studies

A proper suspension of the materials in solution is a key issue for its application. Once isolated, UVM-7 and Ti-UVM-7 loaded with A26 are readily suspended in aqueous solutions without exhibiting signs of agglomeration. It should be noted that this suspension under agitation is achieved without any post-treatment of either the inorganic supports or the supports after loading with A26. This is of particular significance given that the preparation and scale-up of these biopesticides should be uncomplicated. Although the suspensions lack colloidal stability, when subjected to minimal agitation (as occurs in fumigation systems), they remain in suspension. In water, UVM-7 loaded with A26 displays a particle size distribution curve with a volume-weighted mean diameter of 54.8 μm (with a 90% particle volume below 113.8 μm) (Fig. 7a). In an analogous manner, the particle size distribution curve for Ti-UVM-7 loaded with A26 demonstrates a slightly larger particle size, exhibiting a weighted mean diameter of 86.5 μm (with a 90% particle volume below 270.6 μm) (Fig. 7b). These values are adequate for its use in sprayers. We tested its application in a conventional spraying system without appreciation of any obstructions. These characteristics, which are fundamental to its agricultural application, contribute to its efficacy on a large scale.

### Biocidal activity tests

Based on the above data, the non-functionalized UVM-7 material has been selected for field testing. The Ti-UVM-7 material

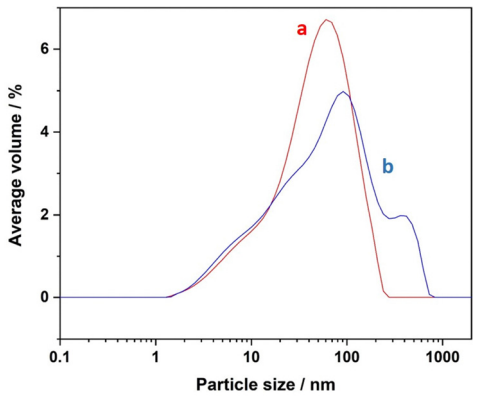


Fig. 7 Particle size distribution curves of (a) UVM-7 and (b) Ti-UVM-7 supports loaded with A26 suspended in water media.

has also been included in the tests to evaluate the protective effect of UV light on the effectiveness of the material. Specifically, tests have been carried out on *Eutetranychus banksi* in citrus.

The eastern mite or eastern red mite is a pest that has recently been detected in the Iberian Peninsula but in a short time has managed to displace other typical pests. The mite mainly colonizes the leaf bundle, and it is located around the central nerve, where the remains of chorions and whitish molts can be observed. It shows a clear preference for sun-exposed surfaces, so these areas of the tree are the most affected. It feeds on the chlorophyll contained in the layer of cells just below the epidermal. This produces a silvery and chlorotic puncture on the leaves and fruits. Fruit discoloration disappears when the ripening process is completed, whether natural or artificial (de-grading), although a delay in ripening is observed in the affected area.

For the test, the product containing the UVM-7 (E3) or Ti-UVM-7 (E4) silica material was compared with the commercial product Zenith (E2), citrulline as a conventional control (E1), and an untreated control (E0). These results are shown in Fig. 8. If the plants are not treated, there is an increased number of mites after 3 and 7 days. Under the conditions of our test, the commercial azadirachtin formulation (E2) maintains a level of incidence close to those measured in day 0 during the seven days of the test but is not able to control *E. banksi*. By contrast, citrulline reduces the degree of incidence to approximately 15% and achieves an effectiveness round 90%. Considering the products containing UVM-7 (E3 and E4), it seems that the encapsulation could improve the effect of azadirachtin. The incidence on day 3 of E3 and E4 is almost half than for E2, and this effect is maintained on day 7. Remarkably, these values are close to the effect observed for the conventional product (E1). Although on day 3, only a tendency is observed, and on day 7, a significant difference is observed with the untreated control.

As can be seen in the severity graph (Fig. 8), the tendency is similar to the one observed in incidence. On day 3, the treatment with biocide only (E2) is able to reduce the number of insects; however, its effect is much lower than with the conventional treatment, with a reduction of only 17% and 68% on

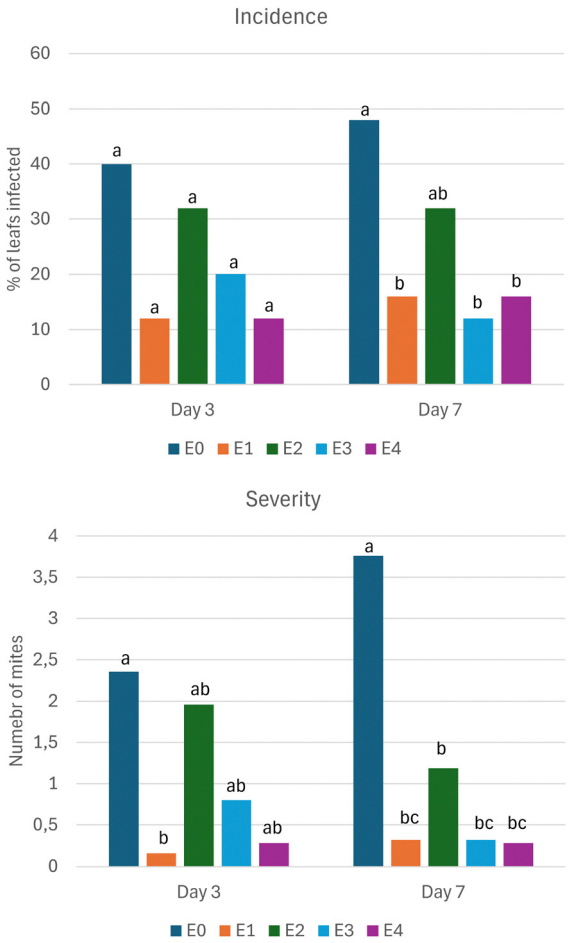


Fig. 8 Evaluation of the effect of the formulations against *E. banksi*. Within each day, treatments with the same latter belong to the same group.

day 3 and 7, respectively. By contrast, the encapsulation in the UVM-7 mesoporous material (E3 and E4) increases the effect, approaching it to the values of the conventional treatment (E1). It seems that loading the active substances could be an effective approach to increase the effectiveness of the essential oils. This effect is more pronounced on day 7. Although the results are promising, the benefits derived from encapsulation are not statistically significant because the encapsulated and non-encapsulated tests are sited in the same group on the two testing dates. If we review the effect of Ti as a UV protector, we observe a beneficial effect on day 3, but there is no difference on day 7. Previously, it has been reported that this type of materials offers a sun protection factor of,[49] a value that can be too low to offer significant UV protection.

## Conclusions

A series of nanomaterials with different shapes, pore sizes and functionalization were prepared for the encapsulation and controlled release of neem oil and azadirachtin-based formulations. These results indicate that the presence of textural porosity in the range of 40 nm and silanol groups at the surface are particularly adequate for the loading of neem oil and formulations, being able to encapsulate up to a 35% of the active substance in the case of UVM-7 materials. The resulting material can modulate release, providing slow release. The encapsulation reduces the incidence and severity of *E. banksi* compared to pure Zenith A26, approaching the levels of conventional citronella treatment. Despite the favourable results, the inclusion of titanium did not improve the long effect of the material and only a partial removal of the plague is achieved. Thus, these types of materials could be an interesting approach towards more sustainable agriculture. Further studies could include field tests with neem oils instead of Zenith A26 or the evaluation of the effect of supports with stronger UV protection.

## Data availability

The authors declare that the data supporting the findings of this study are available within the paper.

## Conflicts of interest

There are no conflicts to declare.

## Acknowledgements

This study was supported by the grants AGCOOP_A/2022/019 funded by the Grants for cooperation of the PDR-C.V 2014-2020 with support from the European Union (European Agricultural Fund for Rural Development), Spanish Ministry of Agriculture, Fishing, Food, and Environment, and Generalitat Valenciana; and by the AGROALNEXT programme supported by MCIN with funding from the European Union Next Generation EU (PRTR-C17.I1) and by the Generalitat Valenciana grant number EUAGROALNEXT/2022/065.

## Notes and references

1 N. K. Arora, S. Mehnaz and R. Balestrini, *Bioformulations for Sustainable Agriculture*, Springer, India, 2016.
2 FAO, 2009. Global agriculture toward 2050, High Level Expert Forum – How to Feed the World in 2050, **https://www.fao.org/fileadmin/templates/wsfs/docs/Issues_papers/HLEF2050_Global_Agriculture.pdf**.
3 Population Institute, 2017. FAO says Food Production must Rise by 70%, Available online at **https://www.populationinstitute.org/resources/populationonline/issue/1/8**.
4 A. Roques, W. Rabitsch, J. Rasplus, C. LopezVaamonde, W. Nentwig and M. Kenis, Handbook of Alien Species in Europe, in *Alien Terrestrial Invertebrates of Europe*, ed. Hulme, P. E., *et al.*, Springer, Amsterdam, 2009, pp. 63–79.
5 J. Jampílek and K. KráĽová, in *Chapter 17 - Nanobiopesticides in agriculture: State of the art and future opportunities*, ed. O. Koul, Nano-Biopesticides Today and Future Perspectives, Academic Press, 2019, pp. 397–447, ISBN 978-0-12-815829-6.

 

6 A. B. Tleuovaa, E. Wielogorska, V. S. S. L. P. Talluria, F. Štěpáneka, C. T. Elliottd and D. O. Grigoriev, *J. Controlled Release*, 2020, **326**, 468–481.
7 J. N. Simons and T. A. Zitter, *Plant Dis.*, 1980, **64**, 542–546.
8 M. B. Isman, *Phytochem. Rev.*, 2020, **19**, 235–241.
9 R. Raveau, J. Fontaine and A. Lounès-Hadj Sahraoui, *Foods*, 2020, **9**, 365.
10 I. E. Popescu, I. N. Gostin and C. F. Blidar, *Agriengineering*, 2024, **6**, 1195–1271.
11 S. Hernández, C. Cabaleiro, J. Jacas and B. Martín, *Boletín de Sanidad Vegetal. Plagas*, 2002, **28**, 223–237.
12 V. López López, C. Cabaleiro Sobrino and B. Martín López, *Cuadernos de Fitopatología*, 2003, **76**, 54–62.
13 B. Martín, V. López and C. Cabaleiro, *Span. J. Agric. Res.*, 2003, **13**, 73–77.
14 B. Martín López, I. Varela Barrenechea and M. Lores Hermida, *Bol. San. Veg. Plagas*, 2004, **30**, 177–183.
15 R. Laborda, I. Manzano, M. Gamón, I. Gavidia, P. Pérez-Bermúdez and R. Boluda, *Ind. Crop. Prod.*, 2013, **48**, 106–110.
16 K. Adhikari, S. Bhandari, D. Niraula and J. Shrestha, *J. Agric. Appl. Biol.*, 2020, **1**, 100–117.
17 G. Brahmachari, *ChemBioChem*, 2004, **5**, 409–421.
18 K. Dhingra and K. L. Vandana, *Int. J. Dent. Hygiene*, 2017, **15**, 4–15.
19 S. Kilani-Morakchi, H. Morakchi-Goudjil and K. Sifi, *Front. Agronomy*, 2021, **3**, 676208.
20 A. Lyubenova, L. Georgieva and V. Antonova, *Biotechnol. Biotechnol. Equip.*, 2023, **37**, 2297533.
21 S. Adusei and S. Azupio, *J. Chem.*, 2022, 6778554.
22 S. J. Boeke, M. G. Boersma, G. M. Alink, J. J. A. van Loon, A. van Huis, M. Dicke and I. M. C. M. Rietjens, *J. Ethnopharmacol.*, 2004, **94**, 25–41.
23 A. Bandoni, *Los recursos vegetales aromaticos en Latinoamerica*, Editorial de la Universidad Nacional de La Plata, Argentina, 2000.
24 S. Chaudhary, R. K. Kanwar, A. Sehgal, D. M. Cahill, C. J. Barrow, R. Sehgal and J. R. Kanwar, *Front. Plant Sci.*, 2017, **88**, 610.
25 E. V. R. Campos, J. L. de Oliveira, M. Pascoli, R. de Lima and L. F. Fraceto, *Front. Plant Sci.*, 2016, **7**, 1494.
26 A. Dominguez, E. Lanchazo, L. Armengol and J. M. Carot, *Uso de fitosanitarios en el control ecológico del minador de los cítricos en plantones de mandarino*, V Congreso de la SEAE.
27 A. Ioannou, G. Gohari, P. Papaphilippou, S. Panahirad, A. Akbari, M. Reza Dadpour, T. Krasia-Christoforou and V. Fotopoulos, *Environ. Exp. Bot.*, 2020, **176**, 104048.
28 S. Kumar, M. Nehraa, N. Dilbaghi, G. Marrazza, A. A. Hassan and K.-H. Kim, *J. Controlled Release*, 2019, **294**, 131–153.
29 R. P. Singh, R. Handa and G. Manchanda, *J. Controlled Release*, 2021, **329**, 1234–1248.
30 T. Li, D. Teng, R. Mao, Y. Hao, X. Wang and J. Wang, *J. Biomed. Mater. Res.*, 2019, **107A**, 2371–2385.
31 S. M. Hosseini, J. Mohammadnejad, S. Salamat, Z. Beiram Zadeh, M. Tanhaei and S. Ramakrishna, *Mater. Today Chem.*, 2023, **29**, 101400.
32 Y. Xu, Y. You, L. Yi, X. Wu, Y. Zhao, J. Yu, H. Liu, Y. Shen, J. Guo and C. Huang, *Bioact. Mater.*, 2023, **20**, 418–433.
33 M. Shellaiah and K.-W. Sun, *Biosensors*, 2022, **12**, 550.
34 P. R. Patel, A. Singam, A. Dadwal and R. V. N. Gundloori, *J. Drug Delivery. Sci. Technol.*, 2022, **75**, 103629.
35 B. D. Mattos, O. J. Rojas and W. L. E. Magalhaes, *J. Cleaner Prod.*, 2017, **142**, 4206–4213.
36 M. Menossi, R. P. Ollier, C. A. Casalongué and V. A. Alvarez, *J. Chem. Technol. Biotechnol.*, 2021, **96**, 2109–2122.
37 M. Bravo Cadena, G. M. Preston, R. A. L. Van der Hoorn, H. E. Townleya and I. P. Thompson, *Ind. Crops Prod.*, 2018, **122**, 582–590.
38 Y. Zhu, C. Li, H. Cui and L. Lin, *Food Control*, 2021, **123**, 107856.
39 F. Gao, H. Zhou, Z. Shen, H. Qiu, L. Hao, H. Chen and X. Zhou, *J. Dispersion Sci. Technol.*, 2020, **41**, 1859–1871.
40 A. Ebadollahi, J. J. Sendi and A. Aliakbar, *J. Econ. Entomol.*, 2017, **110**, 2413–2420.
41 I. Mallard, D. Bourgeois and S. Fourmentin, *Colloids Surf., A*, 2018, **549**, 130–137.
42 M. Pascoli, M. T. Jacques, D. A. Agarrayua, D. S. Avila, R. Lima and L. F. Fraceto, *Sci. Total Environ.*, 2019, **677**, 57–67.
43 M. Ruiz-Rico, E. Oérez-Esteve, A. Bernardos, F. Sancenón, R. Martínez-Mañez, M. D. Marcos and J. M. Barat, *Food Chem.*, 2017, **233**, 238.
44 W. Weisany, S. Yousefi, S. P. Soufiani, D. Pashang, D. J. McClemens and M. Ghasemlou, *Adv. Colloid Interface Sci.*, 2024, **325**, 103116.
45 B. Anjaneyulu, V. Chauhan, C. Mittal and M. Afshari, *J. Environ. Chem. Eng.*, 2024, **12**, 113693.
46 W. Stöber and A. Fink, *J. Colloid Interface Sci.*, 1968, **26**, 62–69.
47 M. D. Garrido, J. El Haskouri, D. Vie, A. Beltrán, J. V. Ros-Lis, M. D. Marcos, N. Moliner and P. Amorós, *Microporous Mesoporous Mater.*, 2022, **337**, 111942.
48 M. Benítez, C. Rodríguez-Carrillo, S. Sánchez-Artero, J. El Haskouri, P. Amorós and J. V. Ros-Lis, *Green Chem.*, 2024, **26**, 785–793.
49 C. Rodríguez-Carrillo, M. Benítez, M. González-Fernández, R. de los Reyes, S. Murcia, J. El Haskouri, P. Amorós and J. V. Ros-Lis, *Microporous Mesoporous Mater.*, 2024, **380**, 113314.
50 G. Esparza-Díaz, J. López-Collado, J. A. Villanueva-Jiménez, F. Osorio-Acosta, G. Otero-Colina and E. Camacho-Díaz, *Agrociencia*, 2010, **44**(7), 821–833.